Seismicity and sedimentation rate effects on submarine slope stability

Article *in* Geology · June 2016

DOI: 10.1130/G37866.1

3 authors, including:

Uri ten Brink
United States Geological Survey
153 PUBLICATIONS **3,243** CITATIONS
SEE PROFILE

Brian D. Andrews
United States Geological Survey
35 PUBLICATIONS **374** CITATIONS
SEE PROFILE

THE GEOLOGICAL SOCIETY OF AMERICA®

Seismicity and sedimentation rate effects on submarine slope stability

U.S. ten Brink[1,2], B.D. Andrews[1], and N.C. Miller[1]
[1]U.S. Geological Survey, Woods Hole, Massachusetts 02543, USA
[2]Department of Marine Geosciences, University of Haifa, Haifa 3498838, Israel

ABSTRACT

We explore the effects of earthquake frequency and sedimentation rate on submarine slope stability by extracting correlations between morphological and geological parameters in 10 continental margins. Slope stability increases with increasing frequency of earthquakes and decreasing sedimentation rate. This increase in stability is nonlinear (power law with $b < 0.5$), accelerating with decreasing interseismic sediment accumulation. The correlation is interpreted as evidence for sediment densification and associated shear strength gain induced by repeated seismic shaking. Outliers to this correlation likely identify margins where tectonic activity leads to relatively rapid oversteepening of the slope.

INTRODUCTION

Large submarine mass-transport scars are commonly observed on continental margins, but they are noticeably less abundant in margins that experience frequent earthquakes compared to those that seldom experience them (Fig. 1; e.g., McAdoo et al., 2000; Urgeles and Camerlenghi, 2013). This is a surprising observation, given that horizontal acceleration from earthquakes and associated strength loss from cyclic loading and liquefaction are commonly thought to provide the primary triggers for inducing failures and subsequent mass movements (e.g., Hampton et al., 1996). Direct evidence for the paucity of scars following the M 9.1 Sumatra (Indonesia) and the M 8.8 Maule (Chile) earthquakes reinforces this observation (Henstock et al., 2006; Völker et al., 2011). Drilling into the Hellenic forearc also encountered far fewer failure events than predicted by earthquake recurrence (Strozyk et al., 2010). The relative paucity of scars in those margins has been explained by lack of available sediments (Tappin et al., 2007), "dynamic compaction," or "seismic strengthening" by earthquakes (Lee et al., 2004; Strozyk et al., 2010).

Here, we compare 10 margins for which we had access to raw multibeam bathymetry data, and which are associated with a range of earthquake recurrences. These are the convergent margins of El Salvador–Guatemala, Nicaragua–northern Costa Rica, Washington State and northern Oregon (USA, north of 45.1°N), southern Oregon, Makran (Pakistan-Iran), northern Sumatra, Muertos (northern Caribbean), the transpressive margin of Queen Charlotte fault at Haida Gwaii (Canada), the rifted margin of southern New England (U.S. Atlantic margin), and Israel. These margins are associated with a range of earthquake frequencies, sedimentation rates, slope gradients, and morphological profiles. To further compare among the margins, we focused the study on scars on the continental slope, ignoring, for example, the many scars found on the continental rise of the U.S. Atlantic margin (Chaytor et al., 2009). The calculated margin area, marked by polygons in Figure DR1 in the GSA Data Repository[1], therefore encompasses the scars from the trench axis (or slope-rise boundary in passive margins) to the shelf edge or the upper edge of the available data (Table 1). We examined correlations across these margins between the fraction of the continental slope that is covered by scars (henceforth, scar fraction) and average sedimentation rates, earthquake recurrence, and slope gradients, in order to understand their effects on slope strength.

METHODS

We processed the raw multibeam bathymetry data from different margins and gridded them at 50–100 m intervals (Fig. 1; Fig. DR1; Table DR1). We examined only large (4500–37,200 km^2) and contiguous regions with along-strike lengths varying between 100 km and 580 km. Scars were identified in the bathymetry data as zones of excavations surrounded, at least partly, by scarps that break the local slopes. Scars were mapped in each area at a map scale of 1:100,000, by examining depth, shaded relief, and gradient maps of the area using ESRI ArcGIS software (www.arcgis.com). A three-dimensional (3-D) rendition of the bathymetry in the Caris EasyView application (www.caris.com/products/easy-view/) was concurrently displayed, rotated, and dynamically shaded from different angles to help with the identification of the scars. Volumes were calculated by subtracting the scar surface from smooth artificial surfaces connecting the tops of the surrounding scarps (for details of the methodology, see Chaytor et al., 2009; ten Brink et al., 2006). Scars along submarine canyon walls likely formed by collapses into deepening channels were ignored. Adhering to this procedure ensured consistent mapping of scars across different environments. Different parameters were extracted from this analysis. They included the margin area, the mean and standard deviation of its slope gradient, the total scar area and volume, the mean gradient of the scars' "missing" surfaces, and the mean scar thickness (Table 1; Table DR2).

We used published statistical analyses of earthquake recurrence for large earthquakes (typically ≥ M7) in Pacific margins (Nishenko, 1991; Goes, 1996; Table DR3). Similar analysis does not exist for northern Sumatra and Makran, but recurrence estimates from historical earthquakes are available (see details in Table DR3). Published estimates are lacking for the Israeli, U.S. Atlantic, and Muertos margins. We assumed that scars on the Israeli margin were triggered

Figure 1. Location of studied continental margins. Individual margin maps are shown in Figure DR1 (see footnote 1).

[1]GSA Data Repository item 2016187, tables and figures providing detailed information of data sources and parameters used in the analysis, and in Figure 2 (but excluding scars and margin areas with gradients <3°), is available online at www.geosociety.org/pubs/ft2016.htm, or on request from editing@geosociety.org or Documents Secretary, GSA, P.O. Box 9140, Boulder, CO 80301, USA.

TABLE 1. MORPHOLOGICAL PARAMETERS, EARTHQUAKE RECURRENCE INTERVALS, AND SEDIMENTATION RATES FOR THE CONTINENTAL MARGINS

Margin name	Water depth range (m)	Mean gradient (°)	Scar fraction	Earthquake recurrence (yr)	Sedimentation rate (cm/k.y.)	Interseismic sediment thickness (cm)
Cascadia North	668–2322	5.4 ± 5.9	0.02	500 ± 75	9.8 ± 1.3	4.9 ± 1.4
Cascadia South	104–3111	5.7 ± 5.3	0.13	500 ± 75	9.8 ± 1.3	4.9 ± 1.4
Guatemala–El Salvador	174–6645	6.9 ± 4.2	0.02	60 ± 15	8.5 ± 4.5	0.5 ± 0.4
Israel	83–1130	2.6 ± 2.1	0.30	2604 ± 1302	66.0 ± 42.0	171.9 ± 196.0
Makran	1226–3369	6.0 ± 6.3	0.05	175 ± 74	70.5 ± 23.3	12.3 ± 9.3
Muertos	297–5579	6.1 ± 5.2	0.06	1855 ± 1232	4.3 ± 2.1	8.0 ± 9.2
Nicaragua	306–5797	6.4 ± 3.9	0.04	75 ± 19	35.0 ± 21.0	2.6 ± 2.2
Queen Charlotte fault	7–1944	8.2 ± 9.2	0.01	100 ± 30	1.0 ± 0.5	0.1 ± 0.1
Northern Sumatra	393–4969	12.3 ± 9.1	0.06	150 ± 50	155.0 ± 25.0	23.3 ± 11.5
U.S. Atlantic margin	463–1962	2.8 ± 1.5	0.53	15,000 ± 5000	13.6 ± 6 (Holocene) 72.5 ± 7.5 (Pleistocene)	203.25 ± 157 1087.5 ± 507.9

Note: For additional morphological parameters and details, see Table DR2 (see text footnote 1).

by earthquakes from the Dead Sea transform, 70–100 km to the east, the recurrence of which has been estimated by Hamiel et al. (2009). Based on modeling the scar area distribution on the U.S. Atlantic margin (ten Brink et al., 2009), we assumed that these were triggered by earthquakes. A recurrence interval of 15 ± 5 k.y. was assigned, given the ages of these scars (10–20 k.y.; Chaytor et al., 2015). Although a large (M_L ~ 7.5) earthquake in A.D. 1751 was originally suggested to have occurred on the Muertos convergent margin, this event was later relocated elsewhere (Bakun et al., 2012). Global positioning system (GPS)–based deformation models of the northeast Caribbean suggest 1–3 mm/yr of convergence across Muertos Trough (Benford et al., 2012). A recurrence interval for the Muertos margin of ~1855 ± 1232 yr was estimated, given a typical displacement of 1.6–2.16 m during a M 7–7.5 earthquake (Wells and Coppersmith, 1994) and 50% coupling.

The relationship between earthquake recurrence and triggering of slope failures may not be uniform across different margins because of variations in magnitude, location, and depth of the earthquakes. Variations in seismic attenuation across margins (e.g., low attenuation of the U.S. margin; Flores et al., 2014), and the increasing proportion of energy released at lower frequencies in giant earthquakes may, however, mitigate some of the differences between the margins, justifying a global approach.

Holocene and late Pleistocene sedimentation rates for the different margins utilized published rates derived from cores located on the open slope in or adjacent to the mapped areas (Tables DR2 and DR3). Core sites within canyons and on the shelf, rise, or trench axis were discarded. Typically, only a few published rates exist for each margin; hence a formal uncertainty cannot be quantified, and instead we used the range of published rates. Dense shelf-edge canyon and rill systems in passive margins channel sediments from the shelf to the deep sea, allowing sediments to bypass the continental slope. We therefore limited our analysis to the parts of the U.S. and Israeli margins where these systems are not developed (Fig. 1; Fig. DR1).

Quantitative correlations between the different parameters (e.g., Fig. 2) were calculated by fitting data with a power law, $f(x) = ax^b$, using a nonlinear least-squares Levenberg-Marquardt solver weighted by uncertainty (Jones et al., 2001). The fit among the models in Figure 2 was evaluated by comparing the root mean square misfit [RMS(e)] between the model and the data. We further examined the consistency of the correlations by applying the jackknife test, in which models are calculated by excluding data from one margin at a time (Fig. DR2).

RESULTS

Scar fraction is positively, and perhaps linearly (b ~ 1), correlated with sedimentation rate (Fig. 2A). This correlation is improved if we use the late Pleistocene sedimentation rate for the U.S. Atlantic margin (65–80 cm/k.y.; Austin et al., 1998) instead of the Holocene rate (13.5 cm/k.y.; Chaytor et al., 2015), because the failures along this margin occurred at the end of a period of higher sedimentation (Chaytor et al., 2015).

A better correlation [in terms of RMS(e)] exists between the scar fraction and earthquake recurrence (Fig. 2B). The longer the recurrence interval is, the higher is the scar fraction. This correlation supports previous qualitative suggestions by Urgeles and Camerlenghi (2013) that fewer scars are observed on margins with high seismic activity compared to margins with low seismic activity. Although there is uncertainty in the recurrence of these margins, jackknife tests indicate that significant correlation exists, even without one of these particular margins.

The correlation between the scar fraction and earthquake recurrence can be further improved when we multiply earthquake recurrence by the sedimentation rate. Figure 2C shows that the scar fraction, F, increases nonlinearly ($b < 1$) with increasing average sedimentary thickness that accumulates during an interseismic interval, ψ (in cm),

$$F = 0.018\psi^{0.32}. \quad (1)$$

Jackknife tests indicate that the power-law exponent b is between 0.17 and 0.43 (Fig. 2C). For the complete data set, $b = 0.32$.

The morphology of convergent margins varies with subduction style (Clift and Vannucchi, 2004). In some subduction zones (e.g., Cascadia North and Makran), sediments are scraped off the subducting plate and are accreted to the forearc wedge, resulting in slope basins punctuated by thrust ridges. Those thrust ridges are steep and are dotted with scars (Fig. DR1). In others (Guatemala–El Salvador and Nicaragua–northern Costa Rica), sediments mostly subduct with the plate, accompanied by erosion of the forearc base, resulting in a constant or convex slope. The northern Sumatra and Muertos morphologies have compound shape with prism thrusts and flat slope basins. To test the effect of intermargin morphotectonic differences on the correlations, we repeated the correlations in Figures 2A–2C, considering only margin areas and scar areas with gradients >3° (see Table DR2). A 3° gradient was used to differentiate between slopes that are likely to develop slope failures and those that would not (Strozyk et al., 2010), although slope failures occur also at lower gradients, especially in passive margins (Table 1). Consideration of only the area steeper than 3° slightly improves the fit of the correlations, particularly for earthquake recurrence (Fig. DR2), but it does not alter the previous conclusion.

DISCUSSION

The correlation in Equation 1 suggests that slope stability increases with increasing frequency of earthquakes and decreasing sedimentation rate. This increase in stability (likely associated with increased sediment shear strength; Morgenstern, 1967) is not linear, accelerating with decreasing interseismic sediment accumulation. Increased slope stability, and related shear strength of continental slope sediments, is evident in the correlation between higher mean

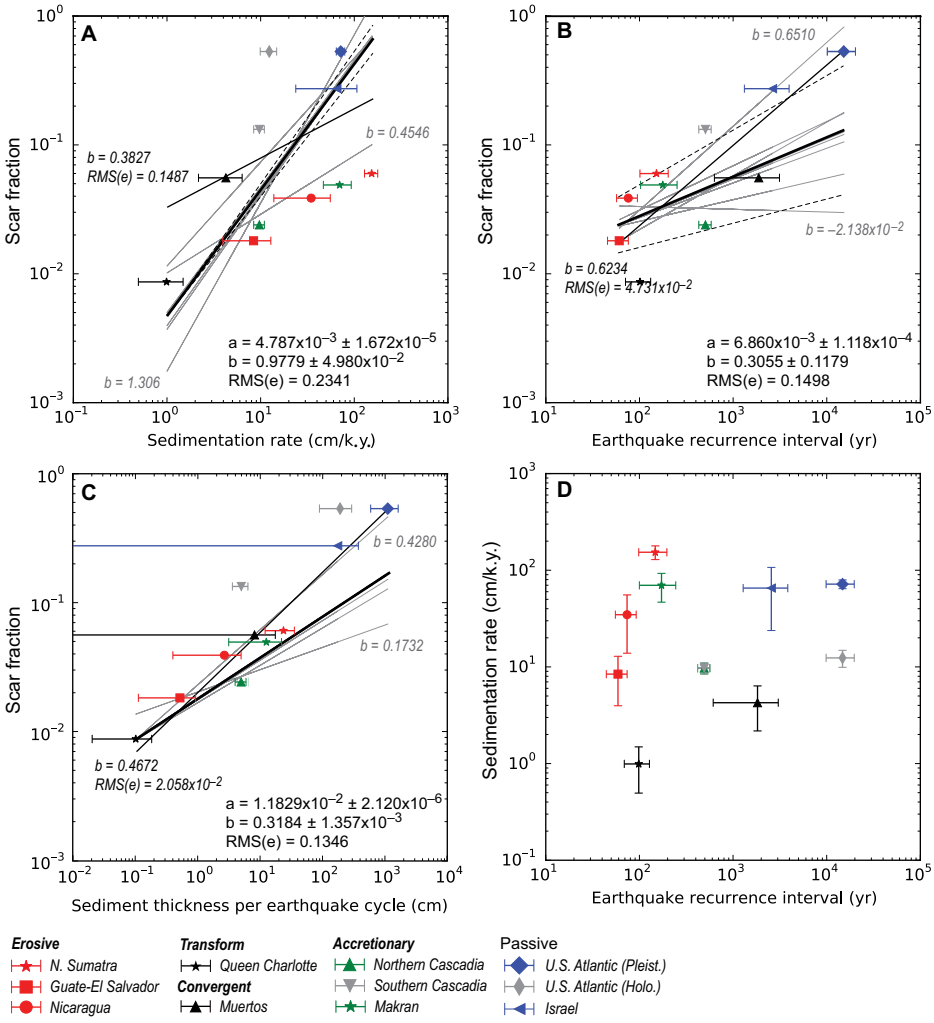

Figure 2. A: Fraction of total margin area covered by scars (scar fraction) for different margins shown in Figure DR1 (see footnote 1) as a function of sedimentation rate. Data and data sources are listed in Tables DR2 and DR3. Estimated range of sedimentation rate is marked by error bars (log scale makes error bars longer on left side of each data point). Heavy solid line is best-fit power law, $f(x) = ax^b$, with parameters *a*, *b*, and RMS(e) listed on bottom right. RMS(e)—root mean square misfit between model and data. Dashed lines show formal uncertainty bounds from covariance matrix. Gray lines are best-fit correlations for various jackknife tests, with minimum and maximum *b* values shown in gray. Thin black line and accompanying *b* and RMS(e) values indicate best-fit correlations, ignoring uncertainty in data, which were used as starting models for nonlinear least-squares (LSQR) solutions with uncertainties. Margins represented by gray symbols were not included in the fit for reasons discussed in the text. B: Same as A, except scar fraction is a function of earthquake recurrence interval. C: Same as A, except scar fraction is a function of sediment thickness that accumulates during an average interval between earthquakes. D: Sedimentation rate as a function of earthquake recurrence interval.

margin slope and increasing earthquake frequency (Fig. 3A). This relationship is apparent in Figure 3B, which shows a generally decreasing scar fraction with increasing margin gradient, similar to McAdoo et al.'s (2000) observations.

Increasing shear strength, induced by horizontal shear strain, has been extensively explored for foundation design and earthquake mitigation on land (e.g., Youd, 1972). Laboratory tests of dry and saturated sand subjected to hundreds of shear strain cycles resulted in sediment densification via a decrease in void ratio (i.e., a reduction in porosity; Youd, 1972), which, in turn was shown to increase the sediment shear modulus (Hardin and Drnevich, 1972). Similar tests in marine sediment are rare. A reconstituted sediment sample from the northern California margin was subjected to bursts of undrained cyclic loading with intermediate periods in which the drainage valve was opened, allowing dissipation of excess pore pressure (Lee et al., 2004). Each burst cycle caused an additional decrease in void ratio and pore pressure, producing apparent overconsolidation (Lee et al., 2004). Shear strength measurements in marine cores corroborate the laboratory results. A measured strength profile in a core located on a stable slope between two large slope failure deposits in Southern California exceeded the expected normally consolidated profile by a factor of 2 or more (Lee et al., 2004). The core probably spans 20 large Holocene earthquakes within the past 5000 yr (Lee et al., 2004). Undrained shear strength values measured in Ocean Drilling Program (ODP) cores from the Japan, Costa Rica, and Cascadia margins are significantly higher than those from the U.S. Atlantic and Amazon margins (Sawyer and DeVore, 2015).

Cyclic loading in the absence of drainage causes reduction in shear strength and even liquefaction, because of increased pore pressure, leading to a decrease in effective stress (Lee et al., 2004). Positive correlation between increased failure and sedimentation rate (Fig. 2A) is an indication that rapid sedimentation is causing underconsolidation, i.e., excess pore pressures generated because the sediment rate is too high to allow full drainage. However, the stronger correlation with earthquake recurrence and with sediment accumulation per earthquake cycle (Figs. 2B and 2C) suggests that the excess pore pressures generated by sedimentation typically have time to dissipate, so that at least normal consolidation prevails, and in sites of frequent earthquakes, the sediment may become overconsolidated, as shown in ODP sites from convergent margins (Sawyer and DeVore, 2015).

Note that the correlation in Equation 1 considers average sedimentation rate and recurrence interval. However, fluctuations in these rates, for example, over glacial-interglacial cycles, can lead to periods of thick sediment accumulation during interseismic cycles, which, according to Figure 2C, will lead to slope failure of large fractions of the margin.

If both sedimentation rate and earthquake recurrence are well constrained, deviations from the correlation in Equation 1 may point to other processes that shape the margin. One likely cause for such deviations is the progressive increase in static shear stress due to increased slope gradient produced by the subduction of an aseismic ridge or a large volcano or by the rise of salt diapirs. In other regions, the cause for steepening may be less clear, although perhaps related to a tectonic mechanism. An example is the southern Cascadia margin off central and southern Oregon (42.25°N–44.85°N), which is similar to the northern Cascadia margin off northern Oregon and Washington in sedimentation rate, earthquake recurrence interval, and average gradient (Table 1), yet the scar fraction is >5.5× larger than for northern Cascadia (Fig. 2C). The scars are particularly abundant along the lower slope of the margin, where the slope is much steeper (10° ± 7°) than in northern Cascadia.

Considering the many factors that could cause deviations from the observed relationship between scar fraction and sedimentation per earthquake interval, it is surprising that such a

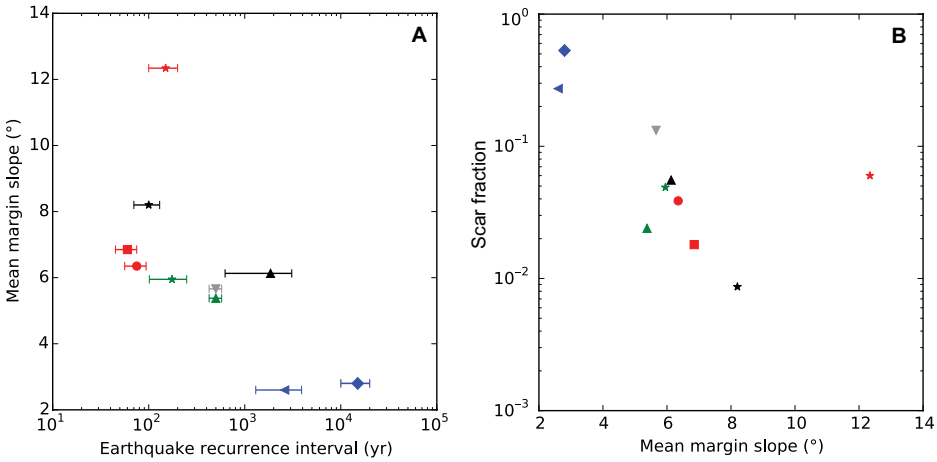

Figure 3. A: Mean margin gradient as a function of earthquake recurrence interval. See Figure 2 for margin symbols. B: Fraction of total margin area covered by scars for different margins shown in Figure 1 as a function of mean gradient of margin.

correlation exists at all. This observation implies that the shape of convergent margins is generally stable over the time scale of several earthquake cycles. Wang and Hu (2006) pointed out that the lower slope of a convergent margin can change its gradient during an earthquake cycle, and this change can promote slope failures. However, our relationship suggests that these changes are generally not cumulative or occur at a rate that is too slow to trigger significant failures.

CONCLUSIONS

A significant correlation exists between the fraction of the continental slope covered by mass-transport scars and sediment accumulation during an interseismic cycle across a range of earthquake frequencies and sedimentation rates. This correlation suggests that earthquake shaking leads to a reduction in the abundance of slope failures, likely by increasing sediment shear strength due to densification. The correlation further suggests that despite tectonic convergence, most convergent margins retain their general slope over many earthquake cycles. Similar work in additional margins should test this hypothesis and help quantify the relationship between scar abundance and earthquake frequency.

ACKNOWLEDGMENTS

We thank Volkmar Leimer, Lisa McNeill, and Vaughn Barrie for providing bathymetry data, and Omri Gadol for sharing his scar picks and associated parameters from Israel. Reviews by Homa Lee, Bill Schwab, Roland von Huene, Jason Chaytor, Celia McHugh, Lisa McNeill, Morelia Urlaub, Rob Kayen, and two anonymous reviewers are gratefully acknowledged.

REFERENCES CITED

Austin, J.A., Jr., Christie-Blick, N., Malone, M.J., et al., 1998, Leg 174A: Proceedings of the Ocean Drilling Program, Initial Reports, Volume 174A: College Station, Texas, Ocean Drilling Program, doi:10.2973/odp.proc.ir.174a.1998.

Bakun, W.H., Flores, C.H., and ten Brink, U.S., 2012, Significant earthquakes on the Enriquillo fault system, Hispaniola, 1500–2010: Implications for seismic hazard: Bulletin of the Seismological Society of America, v. 102, p. 18–30, doi:10.1785/0120110077.

Benford, B., DeMets, C., and Calais, E., 2012, GPS estimates of microplate motions, northern Caribbean: Evidence for a Hispaniola microplate and implications for earthquake hazard: Geophysical Journal International, v. 191, p. 481–490, doi:10.1111/j.1365-246X.2012.05662.x.

Chaytor, J.D., ten Brink, U.S., Solow, A.R., and Andrews, B.D., 2009, Size distribution of submarine landslides along the US Atlantic margin: Marine Geology, v. 264, p. 16–27, doi:10.1016/j.margeo.2008.08.007.

Chaytor, J.D., ten Brink, U.S., Baxter, C.D.P., Brothers, D.S., and Hallam, T.D., 2015, Morphology and age of the southern New England landslide zone: San Francisco, California, American Geophysical Union, Fall Meeting, abstract NH21E–01.

Clift, P. D., and Vannucchi, P., 2004, Controls on tectonic accretion versus erosion in subduction zones: Implications for the origin and recycling of the continental crust: Reviews of Geophysics, v. 42, RG2001, doi:10.1029/2003RG000127.

Flores, C., ten Brink, U.S., McGuire, J., and Collins, J., 2014, Seismicity and attenuation of the continental margin off New York and southern New England from OBS data: San Francisco, California, American Geophysical Union, Fall Meeting, abstract OS33B–1059.

Goes, S.D., 1996, Irregular recurrence of large earthquakes: An analysis of historic and paleoseismic catalogs: Journal of Geophysical Research, v. 101, p. 5739–5749, doi:10.1029/95JB03044.

Hamiel, Y., Amit, R., Begin, Z., Marco, S., Katz, O., Salamon, A., Zilberman, E., and Porat, N., 2009, The seismicity along the Dead Sea fault during the last 60,000 years: Bulletin of the Seismological Society of America, v. 99, p. 2020–2026, doi:10.1785/0120080218.

Hampton, M.A., Lee, H.J., and Locat, J., 1996, Submarine landslides: Reviews of Geophysics, v. 34, p. 33–59, doi:10.1029/95RG03287.

Hardin, B.O., and Drnevich, V.P., 1972, Shear modulus and damping in soils: Journal of the Soil Mechanics and Foundations Division, v. 98, p. 667–692.

Henstock, T.J., McNeill, L.C., and Tappin, D.R., 2006, Seafloor morphology of the Sumatran subduction zone: Surface rupture during megathrust earthquakes?: Geology, v. 34, p. 485–488, doi:10.1130/22426.1.

Jones, E., Oliphant, T., and Peterson, P., 2001, SciPy: Open Source Scientific Tools for Python, v. 0.15.1: http://scipy.org (accessed 24 September 2015).

Lee, H.J., Orzech, K., Locat, J., Boulanger, E., and Konrad, J.-M., 2004, Seismic strengthening, a conditioning factor influencing submarine landslide development, *in* Proceedings of the 57th Canadian Geotechnical Conference (Session 7G): Québec, Canadian Geotechnical Society, p. 8–14.

McAdoo, B., Pratson, L., and Orange, D., 2000, Submarine landslide geomorphology, US continental slope: Marine Geology, v. 169, p. 103–136, doi:10.1016/S0025-3227(00)00050-5.

Morgenstern, N.R., 1967, Submarine slumping and the initiation of turbidity currents, *in* Richards, A.F., ed., Marine Geotechnique: Urbana, Illinois, University of Illinois Press, p. 189–210.

Nishenko, S.P., 1991, Circum-Pacific seismic potential: 1989–1999: Pure and Applied Geophysics, v. 135, p. 169–259, doi:10.1007/BF00880240.

Sawyer, D.E., and DeVore, J.R., 2015, Elevated shear strength of sediments on active margins: Evidence for seismic strengthening: Geophysical Research Letters, v. 42, p. 10,216–10,221, doi:10.1002/2015GL066603.

Strozyk, F., Strasser, M., Förster, A., Kopf, A., and Huhn, K., 2010, Slope failure repetition in active margin environments: Constraints from submarine landslides in the Hellenic forearc, eastern Mediterranean: Journal of Geophysical Research, v. 115, B08103, doi:10.1029/2009JB006841.

Tappin, D., McNeil, L., Henstock, T., and Mosher, D., 2007, Mass wasting processes—Offshore Sumatra, *in* Lykousis, V., et al., eds., Submarine Mass Movements and Their Consequences: Amsterdam, Netherlands, Springer, p. 327–336, doi:10.1007/978-1-4020-6512-5_34.

ten Brink, U.S., Geist, E.L., and Andrews, B.D., 2006, Size distribution of submarine landslides and its implication to tsunami probability in Puerto Rico: Geophysical Research Letters, v. 33, L11307, doi:10.11029/12006GL026125.

ten Brink, U.S., Barkan, R., Andrews, B.D., and Chaytor, J.D., 2009, Size distributions and failure initiation of submarine and subaerial landslides: Earth and Planetary Science Letters, v. 287, p. 31–42, doi:10.1016/j.epsl.2009.07.031.

Urgeles, R., and Camerlenghi, A., 2013, Submarine landslides of the Mediterranean Sea: Trigger mechanisms, dynamics, and frequency-magnitude distribution: Journal of Geophysical Research, v. 118, p. 2600–2618.

Völker, D., Scholz, F., and Geersen, J., 2011, Analysis of submarine landsliding in the rupture area of the 27 February 2010 Maule earthquake, central Chile: Marine Geology, v. 288, p. 79–89, doi:10.1016/j.margeo.2011.08.003.

Wang, K., and Hu, Y., 2006, Accretionary prisms in subduction earthquake cycles: The theory of dynamic Coulomb wedge: Journal of Geophysical Research, v. 111, B06410, doi:10.1029/2005JB004094.

Wells, D.L., and Coppersmith, K.J., 1994, New empirical relationships among magnitude, rupture length, rupture width, rupture area, and surface displacement: Bulletin of the Seismological Society of America, v. 84, p. 974–1002.

Youd, T.L., 1972, Compaction of sands by repeated shear straining: Journal of the Soil Mechanics and Foundations Division, v. 98, p. 709–725.

Manuscript received 8 March 2016
Revised manuscript received 18 May 2016
Manuscript accepted 19 May 2016

Printed in USA

Tables and figures for GSA Data Repository to accompany

Landslides, earthquakes, and sedimentation rate in passive and active margins

By ten Brink, U.S., Andrews, B.D., and Miller, N.C.

Contents

Tables

Figures

Table DR1

Table DR1 – Bathymetry data sources

Margin name	Multibeam bathymetry surveys	Resolution (m)*	Source
Cascadia N. (Washington)	TN265, AVON09MV, MGL1212	50	NOAA-National Centers for Environmental Information
Cascadia N. (Oregon)	Compilation of various surveys	100	NOAA- National Centers for Environmental Information* (http://efh-catalog.coas.oregonstate.edu/bathy/)
Cascadia S. (Oregon)	Compilation of various surveys	100	NOAA- National Centers for Environmental Information* (http://efh-catalog.coas.oregonstate.edu/bathy/
Guatemala-El Salvador	SO173_L2	100	Federal Maritime and Hydrographic Agency of Germany
Israel	Sade et al., 2007	50	Gadol, 2015**
Makran	SO123	100	Federal Maritime and Hydrographic Agency of Germany
Muertos Trough	Compilation of various sources	50	Andrews et al., 2014 (http://pubs.usgs.gov/of/2013/1125/pdf/ofr2013-1125.pdf)
Queen Charlotte Fault	CCGS Vector (Barrie et al., 2013_	10	Canadian Hydrographic Service and Canadian Geological Survey**
Nicaragua-Costa Rica	SO163_L1 &L2, SO144, SO144_L3	100	Federal Maritime and Hydrographic Agency of Germany
Nicaragua-Costa Rica	EW0005, EW0104	100	NOAA- National Centers for Environmental Information
N. Sumatra Trench	HMS Scott (Henstock et al., 2006)	50	National Oceanographic Centre, Southampton, U.K.
U.S. Atlantic Margin	Compilation of various sources	50	Andrews et al., 2013 (http://pubs.usgs.gov/of/2012/1266/appendix_1.html)

Comments:
*The vertical accuracy of the data is ≤ 0.2% of the water depth for a 12 kHz sonar (de Moustier, 2001), the lowest frequency sonar used in this study. It is difficult, however, to quantify the true vertical resolution of the data. A scarp is evident as an abrupt change in slope between pixels. Scarp identification therefore depends on the gradient of the surrounding pixels, the grid size, and the lateral continuity of the scarp.
**All bathymetry data, with the exception of data sources marked by *, were reprocessed using Caris Hips 9.0 from raw line files and the vessel configuration files, cleaned and gridded, following the procedure outlined in Andrews et al., 2013. We used already gridded data sets from Israel (50 m), Queen Charlotte fault (5 m), and Oregon (100 m) because of lack of access to the raw data.

References cited:

Andrews, B. D., Chaytor, J. D., ten Brink, U. S., Brothers, D. S., and Gardner, J. V., 2013, Bathymetric terrain model of the Atlantic Margin for marine geological investigations: U.S. Geological Survey Open-File Report no. 2012-1266.

Andrews, B. D., Uri, S., Danforth, W. W., Chaytor, J. D., Bruña, J.-L. G., Estrada, P. L., and Carbó-Gorosabel, A., 2014, Bathymetric terrain model of the Puerto Rico Trench and the northeastern Caribbean region for marine geological investigations: US Geological Survey Open-File Report no. 2331-1258.

Barrie, J. V., Conway, K. W., and Harris, P. T., 2013, The Queen Charlotte fault, British Columbia: Seafloor anatomy of a transform fault and its influence on sediment processes: Geo-Marine Letters, v. 33, no. 4, p. 311-318.

De Moustier, C., Field evaluation of sounding accuracy in deep water multibeam swath bathymetry, *in* Proceedings OCEANS, 2001, V. 3, IEEE, p. 1761-1765.

Henstock, T. J., McNeill, L. C., and Tappin, D. R., 2006, Seafloor morphology of the Sumatran subduction zone: Surface rupture during megathrust earthquakes?: Geology, v. 34, no. 6, p. 485-488.

Gadol, O., 2015, Submarine slides: shaping of the continental slope offshore Israel, M.Sc. thesis, University of Haifa, 99 pp.

Sade, A.R., Hall, J.K., Amit, G., Golan, A., Gur-Arieh, L., Tibor, G., 2007, The Israel national bathymetric survey - a new look at the seafloor off Israel. Israel Journal of Earth Sciences, v. 55, p. 185–187.

Table DR2

Table DR2- Morphological parameters, earthquake recurrence, and sedimentation rate for the regions bounded by polygons in Fig. DR1

Margin name	Range of water depths (m)*	Margin area (km^2)	Total failure area (km^2)	Total failure volume (km^3)	Mean slide thickness (m)**	Mean margin gradient (°)	% margin > 3°	% scar area > 3°	Scar fraction	Scar fraction >3° ***	Mean slide gradient (°)****	Earthquake recurrence (yr)	Sedimentation rate (cm/ kyr)	Inter-seismic sediment thickness (cm)
Cascadia N	668 - 2322	24171	579	31.56	63	5.4±5.9	54.8	85.2	0.02	0.04	6.9	500±75	9.8±1.3	4.9±1.4
Cascadia S	104 - 3111	12407	1638	109.91	78	5.7±5.3	61.3	87.9	0.13	0.19	8.8	500±75	9.8±1.3	4.9±1.4
Guatemala ElSalvador	174 - 6645	31076	560	42.06	78	6.9±4.2	86.0	90.6	0.02	0.02	6.6	60±15	8.5±4.5	0.5±0.4
Israel[&]	83 - 1130	2256	615	8.92	14	2.6±2.1	31.2	45.1	0.30	0.39		2604±1302	66.0±42.0	171.9±196.0
Makran	1226-3369	8675	424	20.05	54	6.0±6.3	52.5	85.9	0.05	0.08	7.2	175±74	70.5±23.3	12.3±9.3
Muertos	297 - 5579	37191	2065	118.15	63	6.1±5.2	69.0	79.0	0.06	0.06	5.6	1855±1232	4.3±2.1	8.0±9.2
Nicaragua	306 - 5797	14133	546	55.11	108	6.4±3.9	85.0	95.4	0.04	0.04	8.2	75±19	35.0±21.0	2.6±2.2
Queen Charlotte F	7 - 1944	2861	25	0.53	24	8.2±9.2	80.0	97.2	0.01	0.01	12.8	100±30	1.0±0.5	0.1±0.1
N. Sumatra	393 - 4969	19067	1142	61.27	63	12.3±9.1	82.5	96.1	0.06	0.07	14.3	150±50	155.0±25.0	23.3±11.5
U.S. Atlantic	463 - 1962	4538	2407	55.91^	56^^	2.8±1.5	50.7	54.6	0.53	0.57		15000±5000	13.6±6^^^ 72.5±7.5^^^^	203.25±157 1087.5±507.9

Comments:

Average values and uncertainties in columns 12 and 13 are calculated from the range of values listed in Table DR3.

[&]Landslide scars in the Israeli margin were mapped and measured by Gadol (2015).

*Range of water depths includes the slope from the shelf-edge break to the trench axis (in convergent margins) and the rise in non-convergent margins. Bathymetry is unavailable from the uppermost slope of the Makran margin and the wide terrace at the base of the Queen Charlotte Fault margin.

**Mean slide thickness is the total slide volume divided by the total slide area.

***Calculated by dividing that part of the margin area covered by scars with a gradient >3° by the part of the margin area with a gradient >3°.

****Mean slide gradient is the sea floor gradient prior to failure, weighted to slide area. Sea floor gradient prior to failure is calculated by fitting a smooth surface that connects the tops of the slide scarp (see ten Brink et al., 2006; Chaytor et al., 2009 for more details).

^Approximate estimate because of the difficulty of associating scarps with individual scars.

^^Based on total area and volume for the entire U.S. Atlantic margin from Chaytor et al. (2009).

^^^Sedimentation rate for the Holocene.

^^^^Sedimentation rate for the Pleistocene.

References cited:

Chaytor, J. D., ten Brink, U. S., Solow, A. R., and Andrews, B. D., 2009, Size distribution of submarine landslides along the US Atlantic margin: Marine Geology, v. 264, p. 16-27.

Gadol, O., 2015, Submarine slides: shaping of the continental slope offshore Israel, M.Sc. thesis, University of Haifa, 99 pp.

ten Brink, U. S., Geist, E. L., and Andrews, B. D., 2006, Size distribution of submarine landslides and its implication to tsunami probability in Puerto Rico: Geophys. Res. Lett.,, v. 33, L11307, doi:11310.11029/12006GL026125.

Table DR3

TABLE DR3- DATA SOURCES FOR SEDIMENTATION RATE AND EARTHQUAKE RECURRENCE INTERVAL

Margin Name	Sedimentation Rate	Earthquake Recurrence Interval
Cascadia	8.5-11 cm/kyr[1]	500-600 yr[12]
Guatemala – El Salvador	DSDP leg 84: hole 570; 13 cm/kyr[2] (Pleistocene); hole 567 (within a canyon) – 4 cm/kyr[2] (Pleistocene)	M7 – 41-50 yr[13], M7.5 – 40 yr[13]; Northern Nicaragua and El Salvador west of 87°W[12]: 63-91 yr; Guatemala 66-91[12]
Israel	Northern part: 24.7 cm/kyr (last 14.8 kyr)[3]; 29.4 cm/kyr (last 8.8kyr)[3]. Southern part: 24.1 (last 11.6 kyr)[4]; 108 cm/kyr (last 3.7 kyr)[5]	Recurrence is based on the following b-values: Log (N/yr) = 0.97*M+3.67 (Dead Sea Basin) and Log(N/yr) = 0.85M+2.36 (Northern Jordan Valley)[14]. M7 every 1318 yr and 3890 yr, respectively.
Muertos Trough	Core 8: 2.2 cm/ky (last 11,810 yr)[6]; Core 9: 6.4 cm/ky (last 10,610 yr)[6]; Core 9: 5.11 cm/ky (last 30,500 yr)[6]	Maximum displacement for reverse faults log (max. displ.) = -1.84+.29M [15] yields 1.55 m for M7 and 2.16 for M7.5. Assuming 50% coupling, the average displacement per earthquake is expected to be 3.1 m - 4.32 m. Estimated convergence rate across Muertos Trough is 1-3 mm/yr[16]. Hence estimate recurrence interval is: 1855±1232.
Makran	Cores NIOP470 and NIOP471[7] are located within the multibeam bathymetry grid. An age of 8 kyr was identified and marked in these cores[7] by correlation with other dated cores outside the multibeam bathymetry grid. Measured graphically, the marked age is at 68% and 80% of the core length (550 cm and 940 cm respectively), yielding average sedimentation rates of 47 cm/kyr and 94 cm/kyr, respectively.	100-250 yr[7]; 175 yr or longer[21]
Nicaragua – northern Costa Rica	30-40 cm/kyr[8] (Holocene and latest Pleistocene) but with large variations. In detail: Hole M54 - 2 35 cm/kyr (between 15-25 kyr BP), and 13.3 cm/kyr (more recent); Hole M54-3 – 2.2 cm/kyr;	M7 – 53-68 yr[13]; M7.5 – 51-99 yr[13]; Northern Nicaragua –El Salvador west of 87°W: 63-91 yr[12]

	SO173-18 - 90 cm/ky; M66-178 (last 17 kyr) - 16.52 cm/kyr; SO173-11 - 50 cm/kyr	
Queen Charlotte Fault	~0 to 40,000 ^{C}14 yr BP in 3 cores within the fault valley[9] (Vaughn Barrie, written. Comm., 8/24/2015)	70-130 yr[12]; 69 yr[13]; 713 yr for thrust faults but ¼-1/5 of that for strike-slip earthquakes[17]
N. Sumatra	Holocene: 180 cm/kyr[1], also 130-170 cm/kyr[1]	Farther south off Central Sumatra: Super cycles every ~200 yr, 6-8 events caused relative sea level change in the past 700 yr[18] (700/6=118 yr). Northern Sumatra – M7.6 in 1907, M7.2 in 2002, M9.1 in 2004, M7.3 in 2008[19]
U.S. Atlantic margin (Southern New England)	Holocene sedimentation rates[10]: Core 463-2PC 10.8 cm/kyr; 463-15PC - 7.6 cm/kyr; Core 463-16PC – 17 cm/kyr; Core 463-18PC – 9.3 cm/kyr; Core 463-19PC – 19.73 cm/kyr; Core 463-21PC – 11.23 cm/kyr Pleistocene sedimentation rate: Site 1073 (in open slope 60 km south of mapped polygon) >65 cm/ky up to ~80 cm/ky[11];	Landslides are dated at 10,000-20,000[20]. If they were generated by earthquakes, then the last earthquake occurred 15,000±5000 yr ago.

[1]Sumner, E. J., Siti, M. I., McNeill, L. C., Talling, P. J., Henstock, T. J., Wynn, R. B., Djajadihardja, Y. S., and Permana, H., 2013, Can turbidites be used to reconstruct a paleoearthquake record for the central Sumatran margin?: Geology, v. 41, p. 763-766, Data repository and references therein.

[2]Shipboard Scientific Party, 7. Site 570.; Baltuck M., R. von Huene, and R.J. Arnott, 43. Sedimentology of the Western Continental Slope of Central America, in von Huene R., Auboin, J., et al. (eds.), Initial Reports DSDP leg 84 Washington, D.C.

[3]Hammann, Y., Ehrmann, W., Schmiedl, G., Krüger, S., Stuut, J.-B., and Kuhnt, T., 2008, Sedimentation processes in the Eastern Mediterranean Sea during the Late Glacial and Holocene revealed by end-member modelling of the terrigenous fraction in marine sediments: Marine Geology, v. 248, p. 97-114.

[4]Castaneda I. S., Schefuß, E., Pätzold, J., Sinninghe Damsté, J. S., Weldeab, S., and Schouten, S., 2010, Millennial-scale sea surface temperature changes in the eastern Mediterranean (Nile River Delta region) over the last 27,000 years: Paleoceanography, v. 25, PA1208, doi:10.1029/2009PA001740.

[5]Schilman B., Bar-Matthews, M., Almogi-Labin, A., and Luz, B., 2001, Global climate instability reflected by Eastern Mediterranean marine records during the late Holocene: Palaeogeography, Palaeoclimatology, Palaeoecology, v. 176, p. 157-176.

[6]Hoy S. K., Chaytor, J. D., and ten Brink, U.S., 2014, Core data from offshore Puerto Rico and the US Virgin Islands: US Geological Survey Open-File Report no. 2331-1258.

[7]Bourget J., Zaragosi, S., Ellouz-Zimmermann, S., Ducassou, E., Prins, M., Garlan, T., Lanfumey, V., Schneider, J.-L., Rouillard, P., and Giraudeau, J., 2010, Highstand vs. lowstand turbidite system growth in the Makran active margin: Imprints of high-frequency external controls on sediment delivery mechanisms to deep water systems: Marine Geology, v. 274, p. 187-208.

[8]Kutterolf , S., Freundt, A., and Perez, W., 2008, Pacific offshore record of plinian arc volcanism in Central America: 2. Tephra volumes and erupted masses: Geochemistry, Geophysics, Geosystems, v. 9, Q02S03, doi:10.1029/2007GC001826.
[9]Barrie, J. V., Conway, K. W., and Harris, P. T., 2013, The Queen Charlotte fault, British Columbia: Seafloor anatomy of a transform fault and its influence on sediment processes: Geo-Marine Letters, v. 33, p. 311-318.
[10]Chaytor, J. D., ten Brink, U. S., Baxter, C. D. P., Brothers, D. S., and Hallam, T. D., 2015, Morphology and Age of the Southern New England Landslide Zone: AGU Fall Meeting abstract.
[11]Austin, J. A., Jr., Christie-Blick, N., Malone, M. J., et al. 1998, Proceedings of the Ocean Drilling Program, Initial Reports, Vol. 174A Ch. 5, Site 1073A.
[12]Nishenko, S. P., 1991, Circum-Pacific seismic potential: 1989–1999, PAGEOPH, v. 135, p. 169-259.
[13]Goes S. D., 1996, Irregular recurrence of large earthquakes: an analysis of historic and paleoseismic catalogs: Journal of Geophysical Research, v. 101, p. 5739-5749.
[14]Hamiel, Y., Amit, R., Begin, Z., Marco, S., Katz, O., Salamon, A., Zilberman, E., and Porat, N., 2009, The seismicity along the Dead Sea Fault during the last 60,000 years: Bulletin of the Seismological Society of America, v. 99, p. 2020-2026.
[15]Wells, D. L., and Coppersmith, K. J., 1994, New empirical relationships among magnitude, rupture length, rupture width, rupture area, and surface displacement: Bulletin of the Seismological Society of America, v. 84, p. 974-1002.
[16]Benford, B., DeMets, C., and Calais, E., 2012, GPS estimates of microplate motions, northern Caribbean: evidence for a Hispaniola microplate and implications for earthquake hazard: Geophysical Journal International, v. 191, p. 481-490.
[17]Lay, T., Ye, L., Kanamori, H., Yamazaki, Y., Cheung, K. F., Kwong, K., and Koper, K. D., 2013, The October 28, 2012 M w 7.8 Haida Gwaii underthrusting earthquake and tsunami: Slip partitioning along the Queen Charlotte fault transpressional plate boundary: Earth and Planetary Science Letters, v. 375, p. 57-70.
[18]Sieh K., Natawidjaja, D. H., Meltzner, A. J., Shen, C.-C., Cheng, H., Li, K.-S., Suwargadi, B. W., Galetzka, J., Philibosian, B., and Edwards, R. L., 2008, Earthquake supercycles inferred from sea-level changes recorded in the corals of west Sumatra: Science, v. 322, p. 1674-1678.
[19]Kanamori H., Rivera, L., and Lee, W. H., 2010, Historical seismograms for unravelling a mysterious earthquake: The 1907 Sumatra Earthquake: Geophysical Journal International, v. 183, p. 358-374.
[20]ten Brink, U. S., Chaytor, J. D., Geist, E. L., Brothers, D. S., and Andrews, B. D., 2014, Assessment of tsunami hazard to the US Atlantic margin: Marine Geology, v. 353, p. 31-54.
[21]Byrne, D. E., L.R. Sykes, and D.M. Davis, 1992, Great thrust earthquakes and aseismic slip along the plate boundary of the Makran subduction zone, Journal of Geophysical Research, v. 97, p. 449–478.

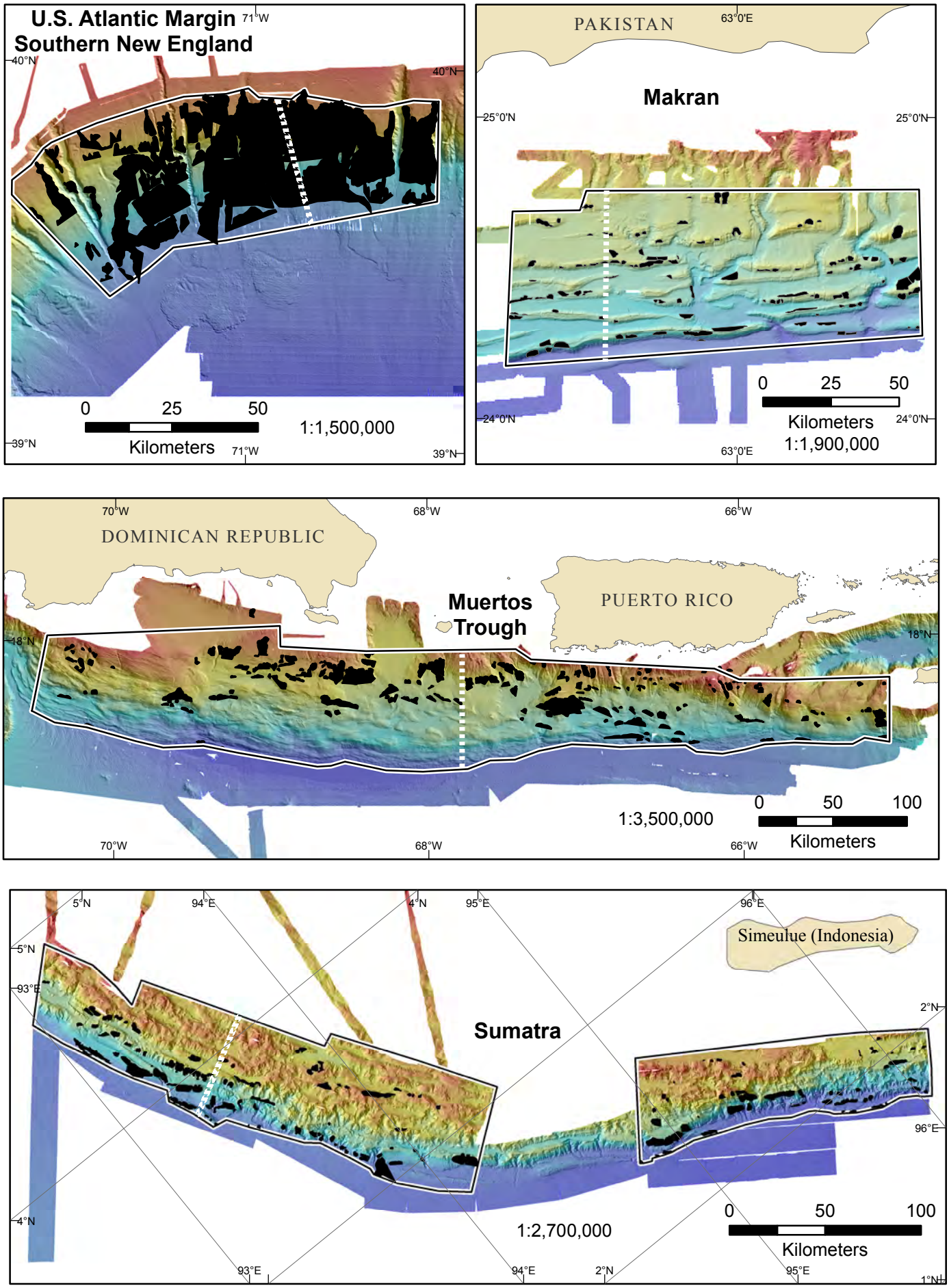
U.S. Atlantic Margin
Southern New England
71°W
40°N
39°N
0
25
50
Kilometers
1:1,500,000
PAKISTAN
63°0'E
Makran
25°0'N
24°0'N
0
25
50
Kilometers
1:1,900,000
70°W
68°W
66°W
DOMINICAN REPUBLIC
PUERTO RICO
Muertos
Trough
18°N
1:3,500,000
0
50
100
Kilometers
5°N
94°E
4°N
95°E
96°E
Simeulue (Indonesia)
93°E
Sumatra
2°N
1°N
1:2,700,000
0
50
100
Kilometers

Figure DR1a

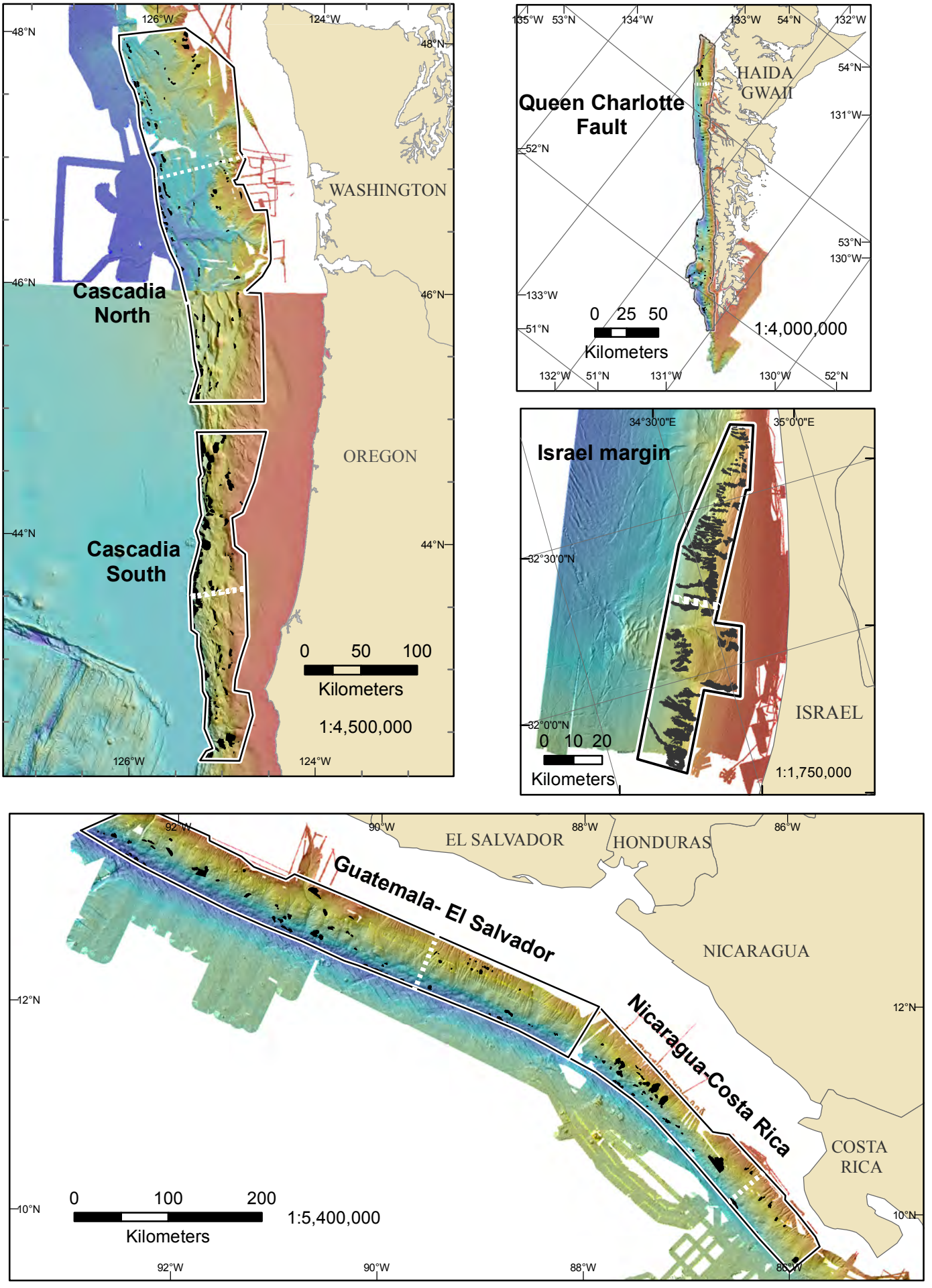
Cascadia North
Cascadia South
WASHINGTON
OREGON
0 50 100
Kilometers
1:4,500,000
Queen Charlotte Fault
HAIDA GWAII
0 25 50
Kilometers
1:4,000,000
Israel margin
ISRAEL
0 10 20
Kilometers
1:1,750,000
Guatemala- El Salvador
Nicaragua-Costa Rica
EL SALVADOR
HONDURAS
NICARAGUA
COSTA RICA
0 100 200
Kilometers
1:5,400,000

Figure DR1b

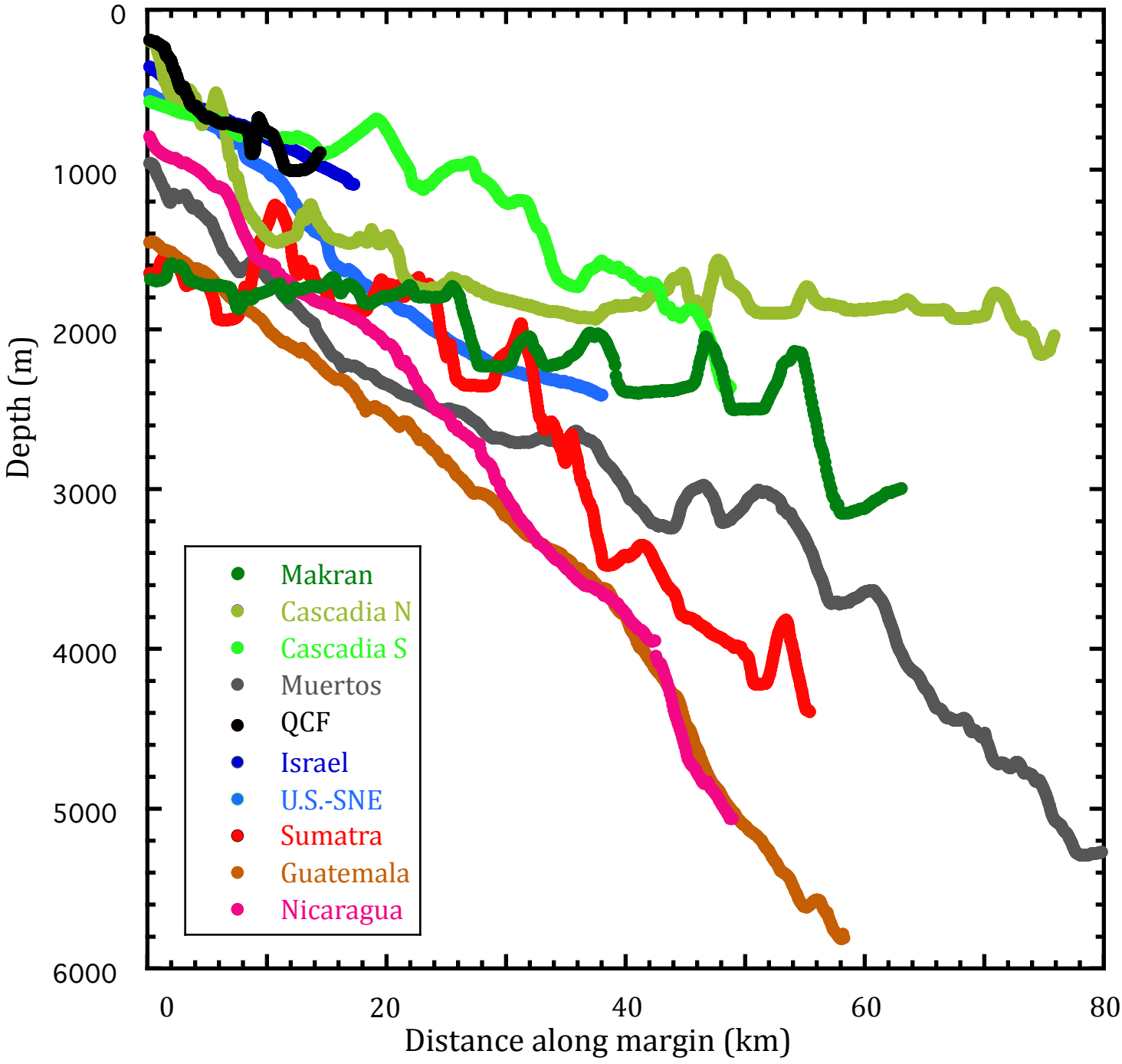
0
1000
2000
3000
4000
5000
6000
Depth (m)
0
20
40
60
80
Distance along margin (km)
Makran
Cascadia N
Cascadia S
Muertos
QCF
Israel
U.S.-SNE
Sumatra
Guatemala
Nicaragua

Figure DR1c

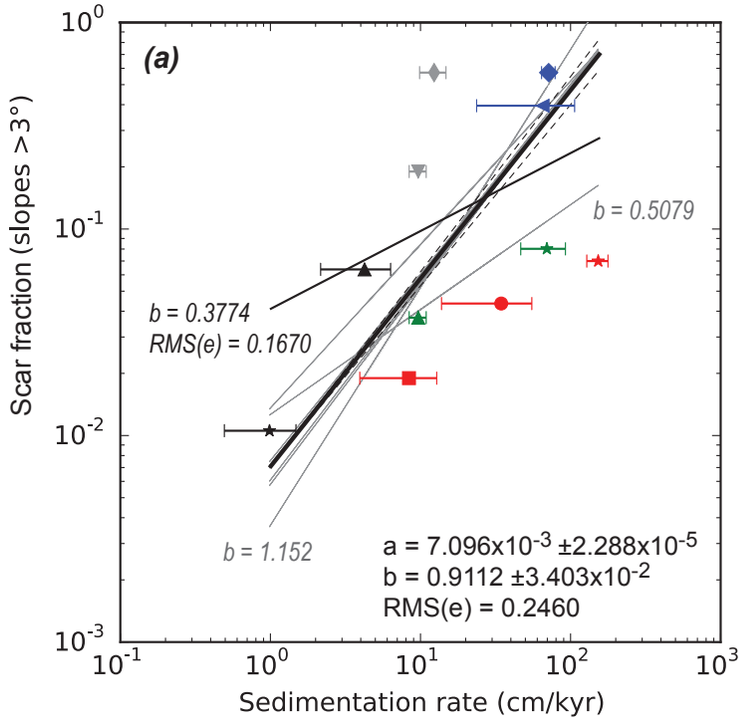

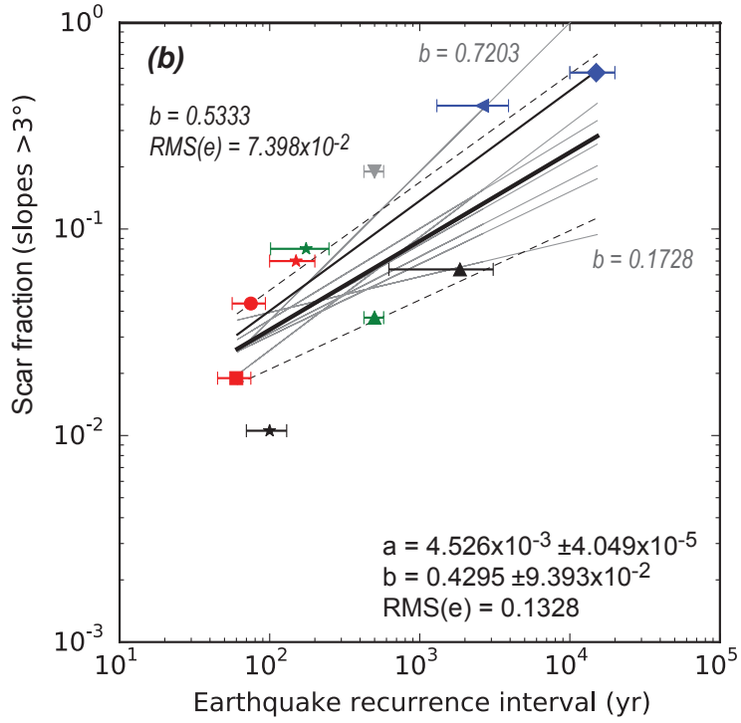

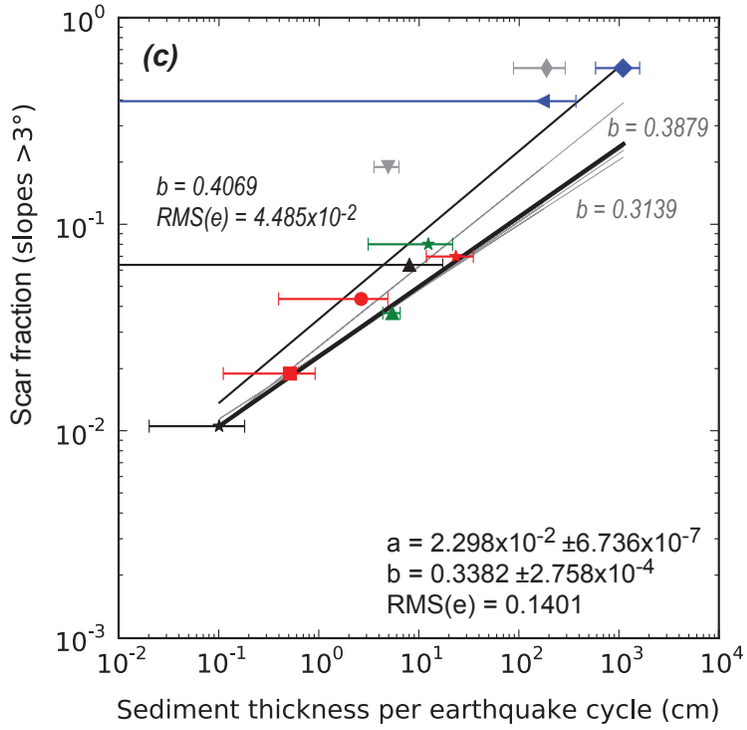

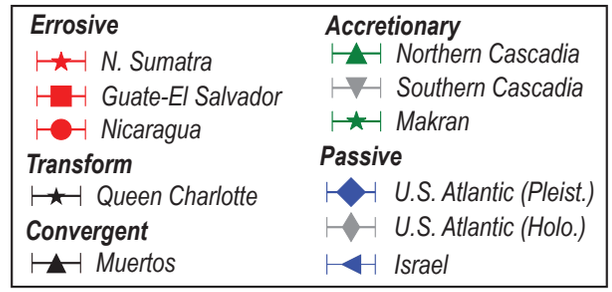

Fig. DR2